ELSEVIER

Polymer 42 (2001) 8055–8067

polymer

www.elsevier.nl/locate/polymer

# Crystallization orientation and relaxation in uniaxially drawn poly(ethylene terephthalate)

X.F. Lu, J.N. Hay*

*Plastic Materials Laboratory, The School of Metallurgy and Materials, The University of Birmingham, Edgbaston, Birmingham B15 2TT, UK*

Received 26 January 2001; received in revised form 11 April 2001; accepted 23 April 2001

**Abstract**

Amorphous polyethylene terephthalate film has been uniaxially drawn below and above the glass transition temperature, $T_g$, and the effect of temperature, strain rate and extent of elongation on the development of crystallinity investigated by differential scanning calorimetry (DSC). The isothermal crystallization time dependence was analysed using the Avrami equation and the mechanism derived was in good agreement with the morphology observed by SEM. Nucleation and growth changed with the degree of strain and there was a change from isotropic spherulites growing uniformly in all directions from randomly oriented nuclei to elliptical spherulites originating from row nuclei and an increased growth rate. The effect of initial orientation on crystallization rate and its dependence on temperature were quantitatively described by Ziabicki's equation.

Changes in molecular orientation on drawing have been measured by polarized FT-IR spectroscopy, based on the ratio of the *trans* to *gauche* conformers of $CH_2$ group in glycol segments. A combination of polarized FT-IR spectroscopy and DSC enabled the degree of orientation in the crystalline and non-crystalline phases to be determined separately. Results indicated that orientation and the strain-induced crystallization increased with increasing draw ratio and elongation, but decreased with increasing temperature in the range of 75–85°C due to the relaxation of molecular chains segments. Relaxation of chain segments mainly occurred in non-crystalline region. © 2001 Elsevier Science Ltd. All rights reserved.

*Keywords*: Poly(ethylene terephthalate); Orientation; Crystallization

## 1. Introduction

Poly(ethylene terephthalate) (PET) is a commercially important engineering polymer whose physical and mechanical properties vary widely with degree of crystallinity, thermal history and orientation. Amorphous PET is of limited commercial significance because of its lower mechanical properties, higher gas permeation rates and lower dimensional stability and sensitivity to physical ageing. However, orientation and crystallization can change the internal morphology of PET and significantly improve these properties.

PET exhibits strain-induced crystallization at a certain orientation level [1–3] and detailed studies been undertaken on the drawing behaviour of PET over the temperature range 20–80°C [4–5]. It was shown that the increase in modulus was due to changes in conformation of the molecular chains, which were extended into the *trans* conformation irrespective of the degree of crystallinity. However, the deformability of PET was affected by the level of strain-induced crystallization [6] and the strength and tensile modulus by the draw ratio. Although there have been some controversy about the effect of orientation and crystallization on properties, it have been confirmed that temperature, strain rate, elongation and molecular weight are the most important variables, which alter the final mechanical and physical properties of PET [7–11].

Although, there have been numerous experimental studies and modelling on strain-induced crystallization of PET [12–20], most of them have been concerned with the change in crystallization of oriented amorphous PET on annealing, or in super-cooled oriented melts but none have monitored the development of crystallinity during deformation nor quantitatively described the effect of the degree of orientation on melt crystallization rates. In previous studies, strain-induced crystallinity has often been measured from density measurement [9,10,21,22]. However, the observed density is not a direct measure of crystallinity but includes a contribution from the degree of chain orientation within the amorphous phase on deformation [10]. Density overestimates

* Corresponding author. Tel.: +44-121-414-4544; fax: +44-121-414-5232.

*E-mail address:* j.n.hay@bham.ac.uk (J.N. Hay).

0032-3861/01/$ - see front matter © 2001 Elsevier Science Ltd. All rights reserved.
PII: S0032-3861(01)00295-6

the level of crystallinity of oriented samples [23]. Light scattering has also been used to characterize spherulite size and shape while morphological changes [9,14,24] and structural models have been derived from small- and wide-angle X-ray diffraction, birefringence studies and anisotropy measured by IR spectroscopy but dissimilar models have been proposed for the structures present in the same polymer system, all based on the same information.

Direct examination of the internal structure of the oriented crystalline polymer sample is necessary to elucidate morphology, but this has been hampered by the lack of the suitable techniques for sample preparation. Although chemical etching is usually employed in preparing samples for SEM investigation, a suitable chemical regent and etching conditions are very crucial for a particular polymer system.

In addition to its use in following changes in the degree of crystallinity, WAXS has been applied to measuring orientation of the crystalline phase, and birefringence to measure the overall orientation of crystalline and amorphous regions [9,10,25]. It is not possible to measure the degree of orientation and conformation change of the two independently due to the large differences in the degree of order between the two regions and competing effects of molecular orientation, relaxation and crystallization. Havens et al. [26] found using multiple pulse dipolar decoupling techniques that three domains, i.e. crystalline, oriented meso- and amorphous phases were present in an oriented sample each with very different chain segment mobilities. On investigating the drawing behaviour of semicrystalline PET, Dargent [27] confirmed the coexistence of a completely disordered amorphous and an ordered mesomorphic phase by comparing DSC, wide-angle X-ray diffraction and birefringence analysis of the samples. Neither birefringence nor X-ray diffraction measurements gave any information on the structural or conformation changes occurring on drawing. These techniques could only detect the intermediate non-crystalline phase, which occurs simultaneously with strain-induced orientation and crystallization [28,29].

Various IR spectroscopic techniques have the ability to measure the degree of orientation and examine structural changes associated with the drawing of PET [30,31], but the complex tilting of the specimen is required to obtain transmission values in the sample thickness. In addition, thin film samples ($<$0.02 mm) are necessary because of the strong absorption of most molecular bands. Attenuated total reflection (ATR) has been used to measure surface orientation of PET [32,33], but differences between surface and bulk were observed, presumably due to inhomogeneity on the surface. Another limitation of this analytical technique has been the uncertainty of the contact between the sample and the high refractive index crystal, which would reduce the reproducibility of results. There is no sample–crystal contact problem or thickness limitation with polarized external specular reflection spectroscopy [34]. However, in order to obtain reproducibility during the hot-drawing of PET at 80°C, Ajji et al. [29] emphasized that a correlation between surface and bulk was necessary, since the physical state of the surface was different from the bulk when surface irregularities were present. Specular reflection techniques have been well established to measuring orientation and obtaining structural information for uniaxially drawn PET [35–37] and a quantitative correction for the surface inhomogeneities in the overall orientation function has been made. Finally, good correlation has been obtained between modulus, crystallinity and the degree of orientation.

Difficulties have arisen in understanding the changes that accompany the drawing of a polymer between the competing mechanisms of orientation, crystallization and molecular relaxation and the dependence of these on temperature, strain and strain rate. Although, there have been several analyses of molecular chain relaxation in drawn PET [38–41] in order to get a thorough understanding of the overall behaviour, a more in-depth investigation is required. In this study, alternative methods have been used to measure orientation in the crystalline and non-crystalline phases separately, the degree of crystallinity and conformation of molecular chain segments during drawing. The effect of temperature, strain and strain rate on the development of crystallinity, molecular orientation, and relaxation have been extensively explored during the drawing of amorphous PET film.

## 2. Experimental

Commercial PET was obtained from ICI. The viscosity average molecular weight was 16.0 kg mol$^{-1}$ and polydispersity 2.2. PET was dried in vacuo at 100°C for 24 h and then compression moulded at 290°C in a heat press into plaques that were quenched into ice water. Rectangular specimens (1 cm in width, 3.2 cm in length, 1.5–2.0 mm in thickness) were cut directly from these.

Commercial PET film, 13 μm thick, was obtained from Goodfellows. These were stress relieved by melted between metal plates and quenched in ice water to produce amorphous film of thickness 13–20 μm.

Samples were stretched uniaxially at several different temperatures, above and below the $T_g$, on the Minimat extensometer equipped with an environmental chamber. Extension rates of 2–10 mm min$^{-1}$ were performed at preset temperatures. The initial separation between the two jaws was 1 cm. To avoid shrinkage and freeze orientation following drawing, samples were held under load and cooled to room temperature.

The weight fraction crystallinity was determined using a Perkin–Elmer differential scanning calorimeter, model DSC-2 at a scan rate of 20 K min$^{-1}$ under nitrogen. High purity indium (99.999%) was used to calibrate the thermal response of the calorimeter. The spherulitic texture of the specimen was examined using a scanning electron

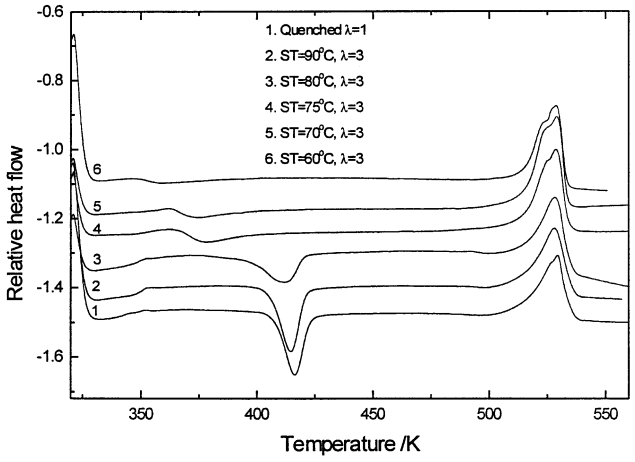


Fig. 1. DSC traces of PET drawn to $\lambda = 3$ at different temperatures compared with an undrawn amorphous sample at 20 K $min^{-1}$.

microscope, Model Jeol 5410 and S-4000. Potassium hydroxide/methanol solution and *n*-propylamine were used to etch the surface of the specimens. All specimens were coated with gold and a silver paint adhesive to make good electrical contact between the specimens and the metal sample holder. This was required to reduce charging-up effects on exposure of the specimens to the electron beam.

FT-IR spectra were measured using a Nicolet Magna-IR 760 ESP spectrophotometer. All spectra were recorded at a resolution of 4 $cm^{-1}$and total of 256 scans were accumulated for each and along with background. Polarization of the IR beam was produced using a zinc selenide wire grid polarizer from Nicolet Ins. Spectra were recorded with the plane of polarization both parallel and perpendicular to the drawn direction. Peak heights were measured by using 'peak height tool' of the 'Omnic' software.

## 3. Results and discussions

### 3.1. Strain-induced crystallization

It was not possible to follow the development of crystallinity during drawing, and so the strain-induced crystallization was investigated by monitoring the post-crystallization. Rectangular PET specimens were drawn to a draw ratio, $\lambda = 3.0$ using a strain rate of $3.3 \times 10^{-3}$ $s^{-1}$ at different temperatures above and below $T_g$ and then quenched to ambient temperature. The subsequent DSC scans, as well as that of an amorphous undrawn PET, are all shown in Fig. 1. PET samples drawn below $T_g$ exhibited less residual crystallization on subsequent heating. While those drawn above $T_g$ were largely amorphous. Typically, PET extended to 200% at 90°C, the subsequent crystallization exotherm observed in DSC was similar to that of the amorphous, undrawn PET. Some orientation remained within the specimen upon drawing, since the crystallization exotherm occurred at a lower temperature than in the undrawn sample. In other words, drawing above $T_g$ produced some orientation but no crystallization, drawing to the same extent below $T_g$ produced some crystallinity represented by the presence of little or no crystallization exotherm on subsequent heating. Others [42,43] have observed similar effects and have assumed that the glass retains on drawing below $T_g$ most of the molecular orientation while above $T_g$, the molecular segments have sufficient mobility to relax. It have been found that the half-life for PET crystallization on drawn at 90°C at strain rate 10 $s^{-1}$ to $\lambda = 4$ is of the order of tens of seconds [44], while the relaxation time of molecular chain segments at this temperature is of the order of $10^{-3}$ s [45]. Furthermore, if the temperature of drawing is sufficiently high, i.e. above 90°C and the strain rate is low enough, i.e. $<1$ $s^{-1}$ [42], 'flowing drawing' occurs and crystallization is not accelerated. Qian et al. [46] have suggested that in such hot-drawn amorphous PET, the macromolecular chains are apparently oriented to a large extent in the global sense, while the local segments have random orientation due to a much faster relaxation rate of chain segments compared with global macromolecular chains. Fig. 1 reflects this trend, in that the crystallization extent with drawing temperatures at a given strain rate, $3.3 \times 10^{-3}$ $s^{-1}$. A separated study on cold- and hot-drawing was made.

Cold-drawing was carried out at 60°C at a strain rate of $3.3 \times 10^{-3}$ $s^{-1}$. Subsequent DSC traces are shown in Fig. 2. In contrast with the amorphous undrawn specimens, crystallinity developed rapidly at a strain $\lambda = 2$ such that only a small amount of residual crystallinity was found on subsequent heating. No further crystallinity developed above a strain of 2 and the strain-induced crystallization was complete within 5 min. Similar investigations have been made by Nobbs [25], Gilli et al. [47] and Göschel [48] who reported that chain segments in the *trans* conformation crystallize below $T_g$.

Thin films were hot-drawn at 75°C at strain rates of $3.3 \times 10^{-3}$ and $17 \times 10^{-3}$ $s^{-1}$ to various strains and subsequently heated in the DSC. The exotherms corresponding

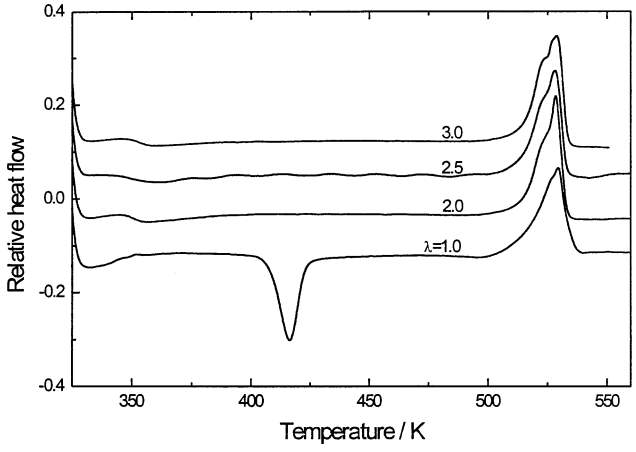


Fig. 2. DSC scans at 20 K $min^{-1}$ on PET samples after cold-drawing at 60°C at strain rate $3.3 \times 10^{-3}$ $s^{-1}$ to different draw ratios.

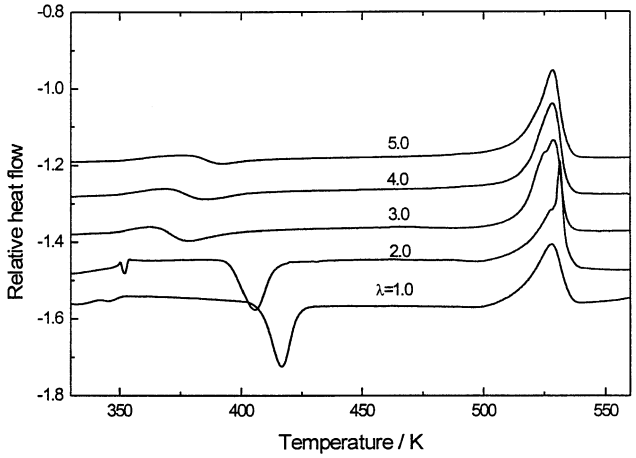


Fig. 3. DSC scans of PET at 20 K $min^{-1}$ after hot-drawing at 75°C at strain rate $3.3 \times 10^{-3}$ $s^{-1}$ to different ratios.

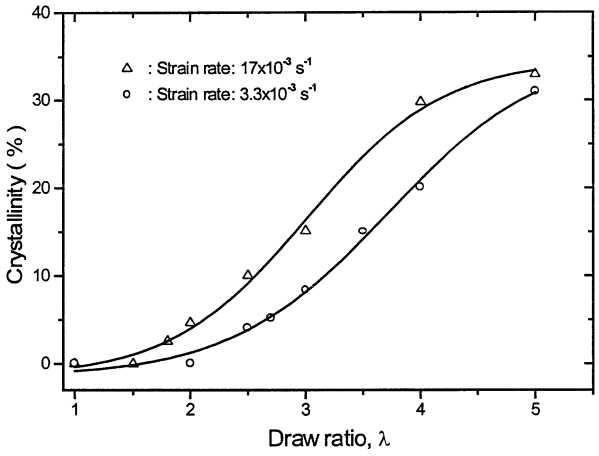


Fig. 5. The development of crystallinity on drawing at 75°C with different strain rates.

to the subsequent crystallization of the drawn sample gradually decreased with increase in draw ratio as can be seen from Figs. 3 and 4. The development of crystallization depended on draw ratio, see Fig. 5, in that samples drawn to $\lambda = 2.5$ at strain rate $3.3 \times 10^{-3}$ $s^{-1}$ and $\lambda = 1.5$ at strain rate $17 \times 10^{-3}$ $s^{-1}$ were amorphous [49] but crystallinity developed on stretching beyond these draw ratios. Even lower strain rates delayed the development of crystallization but similar levels of crystallization were eventually achieved. Salem [43] has reported that reducing the strain rate increased the time available for molecular relaxation to occur and a higher draw ratio was required to attain a degree of orientation at which crystallization can occur. These results are in good agreement with those of Salem's carried out at relatively higher temperatures (83–132°C). They also correlated with Ajji's results at 80°C on PET [35,37].

Drawing was also carried out at 85°C at a strain rate of $17 \times 10^{-3}$ $s^{-1}$, see Fig. 6, and up to $\lambda = 3$, the measured glass transition temperature for drawn PET was constant at the same value as that of the undrawn sample. Above $\lambda =$ 3, the crystallization exotherm shifted to lower temperatures and the peak area decreased. The induction time for the post-crystallization became shorter and the extent of strain-induced crystallization during prior drawing increased. However, strain-induced crystallinity developed very slowly at this temperature, as can be seen from the development of crystallinity with time at constant temperature for variously oriented samples. As also can be seen in Fig. 7, drawing at this temperature produced a slow development of crystallinity and at $\lambda = 7$, only 15% crystallinity was reached. This was very much less than the degree of crystallinity that undrawn PET can achieve (about 32%). This result suggests that the molecular segments have greater mobility and orientation will be inhibited by relaxation at temperature above $T_g$, especially at low strain rates. Therefore, increasing temperature shifts the onset of crystallization to higher draw ratio.

In conclusion, the onset of crystallization on drawing PET depends on the temperature as well as strain rate in that higher temperatures not only enhance the rate of

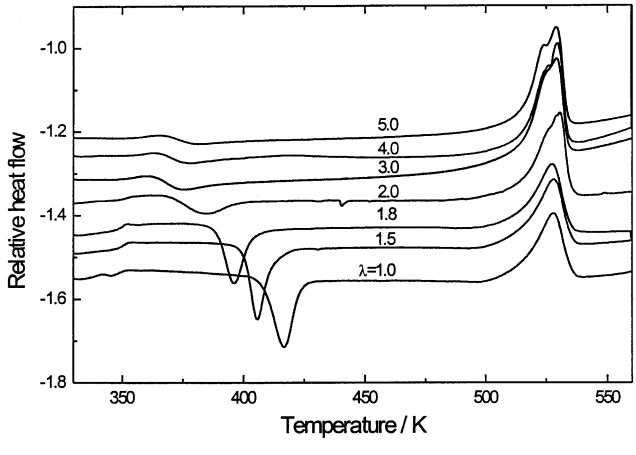


Fig. 4. DSC scans of PET at 20 K $min^{-1}$ after hot-drawing at 75°C at strain rate $17 \times 10^{-3}$ $s^{-1}$ to different ratios.

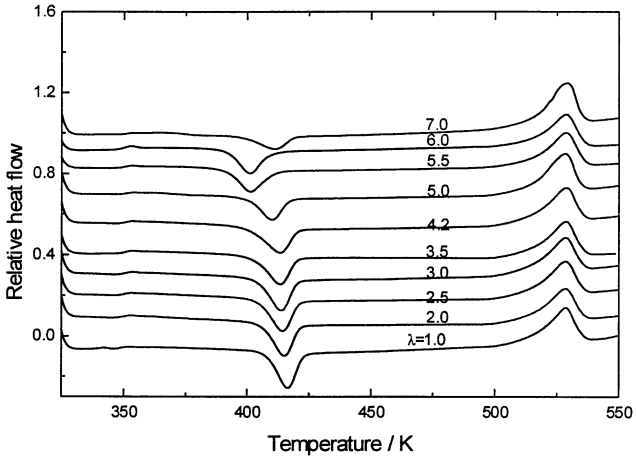


Fig. 6. DSC scans of PET at 20 K $min^{-1}$ after hot-drawing at $17 \times 10^{-3}$ $s^{-1}$at 85°C to different ratios.

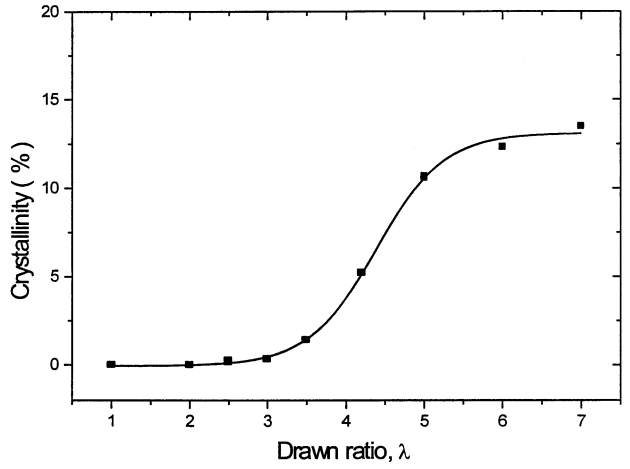


Fig. 7. Development of crystallinity for PET drawing at 85°C and strain rate $17 \times 10^{-3}\ s^{-1}$.

molecule relaxation, but also increases the rate of crystallization at the same level of orientation. Thus, when the time available for molecule relaxation is shorter, at higher strain rates, orientation induces crystallization. Furthermore, once crystalline regions are established, segmental relaxation slows down since the crystallites act as entanglements and temperature and strain rate effects on strain-induced crystallization become increasing complex.

### 3.1.1. Strain-induced isothermal crystallization

PET specimens were drawn to different draw ratios at 85°C, and then crystallized isothermally at 117°C. The crystallization exotherms are shown in Fig. 8. It is evident that with the increase in draw ratio, the overall crystallization shifted to shorter time.

The isothermal crystallization rates were analysed using the Avrami equation [51,52] relating the fractional crystallinity, $X_t$, to time, $t$, by a composite rate constant, $Z$, and the exponent, $n$, i.e.

$$1 - X_t = \exp(-Zt^n) \tag{1}$$

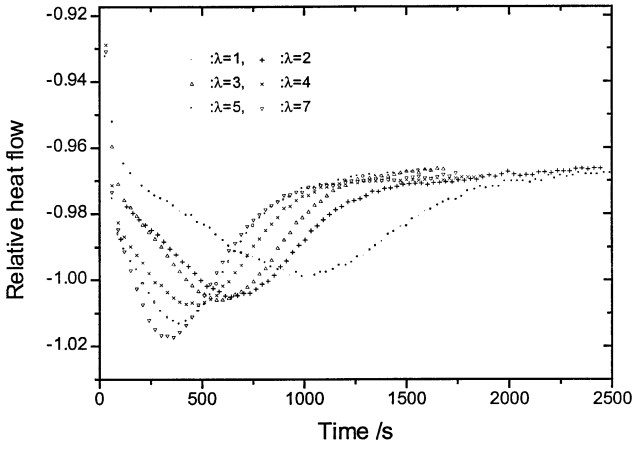


Fig. 8. PET crystallization at 117°C after drawing at 85°C to different extents and comparison with undrawn sample.

The values of $n$ is characteristic of the crystallization mechanism for polymer [53]. $n$ was determined from the slope of the linear plot of $\log[-\ln(1 - X_t)]$ against $\log t$, $X_t$ having been determined from the fractional area of the exotherm from $t = 0$ to $t$. $\ln Z$ was determined by extrapolation of the plot to $t = 1$.

The values of $n$ and $Z$ together with half-life for the crystallization are listed in Table 1. It is clear that the Avrami index for amorphous, isotropic PET ($\lambda = 1$) is $2.5 \pm 0.2$, consistent with growth and impingement of spherulites crystals from heterogeneous nuclei. In comparison, the value of $n$ for oriented PET decreased progressively from 2.5 to 1.6 with the increasing draw ratio consistent with a change in mechanism of crystallization. The crystallization half-life decreased with draw ratio indicating that increased draw ratios lead to faster crystallization rates.

To date, there is no completely successful model to describe strain-induced crystallization kinetics. Empirically, Ziabicki [54] has shown for the case of uniaxial deformation, the effect of orientation on crystallization rate in terms of the half-lives, i.e.

$$\frac{1}{t_{1/2}(f_a)} = \frac{1}{t_{1/2}(0)} \exp(Af_a^2 + Bf_a^3 + \cdots) \tag{2}$$

$t_{1/2}(f_a)$, $t_{1/2}(0)$ represent the half-life for strain-induced crystallization and crystallization that with no orientation, respectively. $f_a$ is the average Herman factor, and A and B the empirical coefficients. For small degrees of orientations, the higher terms in the equation can be neglected and

$$\frac{1}{t_{1/2}(f_a)} = \frac{1}{t_{1/2}(0)} \exp(Af_a^2) \tag{3}$$

A plot of $\ln[1/t_{1/2}(f_a)]$ against $f_a^2$ was linear over a limited range of $f_a^2$ values as can be seen from Fig. 9, and deviations occurred at high orientation and above 5% crystallinity, presumably due to ignoring the higher terms in the exponential, i.e. the coefficient $B$ and even higher terms. But it was also due to the formation of the crystal network reducing the molecular chain mobility.

The coefficient $A$ describes the sensitivity of crystallization rate to the orientation factor, $f_a$ and its value increased almost linearly with increasing temperature, over the limited range investigated, see Fig. 10. From a thermodynamic point of view, the free energy of formation of the critical nuclei for crystal growth rate and nucleation in an oriented melt incorporates an additional term for the entropy decrease of the oriented over that of the unoriented melt, i.e.

$$-\Delta S_e = 1/2NR(\lambda^2 + 2/\lambda - 3) \tag{4}$$

for uniaxial elongation [53].

The free energy difference between the oriented and unoriented melt on crystallization is

$$\Delta G_e = -T\Delta S_e = 1/2NRT(\lambda^2 + 2/\lambda - 3) \tag{5}$$

The linear increase of the sensitivity of the crystallization

Table 1
Parameters for PET drawn at 85°C and crystallized at 117°C

| | Drawn ratio, $\lambda$ | | | | | |
|---|---|---|---|---|---|---|
| | 1 | 2 | 3 | 4 | 5 | 7 |
| Avrami index, $n \pm 0.1$ | 2.5 | 2.1 | 2.0 | 1.6 | 1.7 | 1.5 |
| Rate constant, $Z$ ($\times 10^{-4}$ min$^{-n}$) | 7.02 | 38.0 | 65.3 | 195 | 284 | 389 |
| Half-life, $t_{1/2}$ (min) | 15.3 | 11.9 | 10.3 | 8.17 | 7.37 | 6.82 |

half-lives to the orientation factor, $f_a$, with temperature is consistent with Eq. (5).

### 3.1.2. Changes in crystalline morphology

Heat treatment of the drawn specimens above $T_g$ produced symmetrical spherulites, while those drawn below $T_g$ produced elliptical spherulites with the long axes perpendicular to drawing direction, see Fig. 11a and b, respectively, and are consistent with similar observations made by others [53,54]. This change in spherulitic texture also corresponded with a decrease in the value of the Avrami exponent, $n$, with degree of orientation. The texture of material drawn uniaxially at 60°C to $\lambda = 3$ at a strain rate of $17 \times 10^{-3}$ s$^{-1}$ with a measured crystallinity 29% can be seen in Fig. 12a. After chemical etching, there are strip-like structures aligning more and less perpendicular to the draw direction. For comparison, undrawn amorphous material crystallized at 140°C, and etched under the same conditions, see Fig. 12b, does not show this alignment.

Similarly Stein et al. [14], who studied the development of light scattering patterns on drawing PET at 80°C observed rod-like superstructure with the rods oriented perpendicular to the stretching direction existing at low elongation (40–80%). At higher elongations (115–175%), ellipsoidal spherulites with their long axes perpendicular to the stretching direction appeared. They have considered that the ellipses grew from oriented rod nuclei normal to the drawing direction. It would appear that in essence these rods are the same as the texture observed above. Both chain-extended [56], and shish-kebabs [57,58] structures have been postulated.

### 3.2. Orientation study

Since the development of crystallinity on drawing results as a compromise between orientation and relaxation and is affected by temperature, strain rate and the strain. The degree of orientation of the samples as well molecular conformation was measured on uniaxially drawing.

For the uniaxially drawn specimens, a single dichroic ratio was defined as

$$D = \frac{A_{\parallel}}{A_{\perp}} \tag{6}$$

where $A$ is the absorbance of the IR band with parallel and perpendicular crossed polarizers. The dichroic method can be related quantitatively to certain orientation functions characteristic of the average orientation of the structure unit within the polymer sample, e.g. the Herman orientation function:

$$\langle P_{\alpha}(\cos\theta)\rangle = \frac{D-1}{D+2} \times \frac{2}{3\cos^2\alpha - 1} \tag{7}$$

where $\alpha$ is the angle between the transition dipole moment vector of a particular vibration mode and the chain axis.

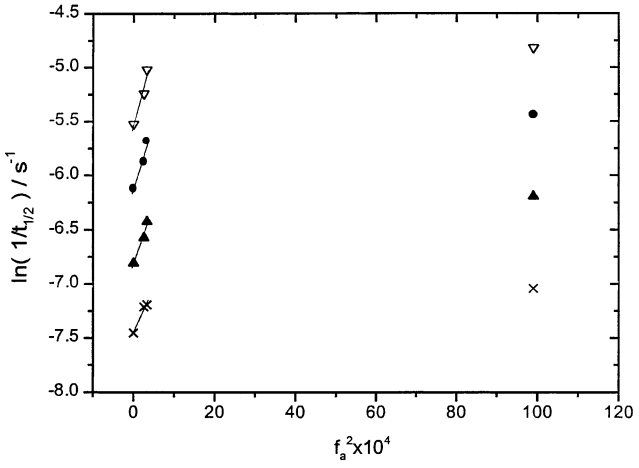


Fig. 9. $\ln[1/t_{1/2}(f_a)]$ against $f_a^2$ at different temperatures.

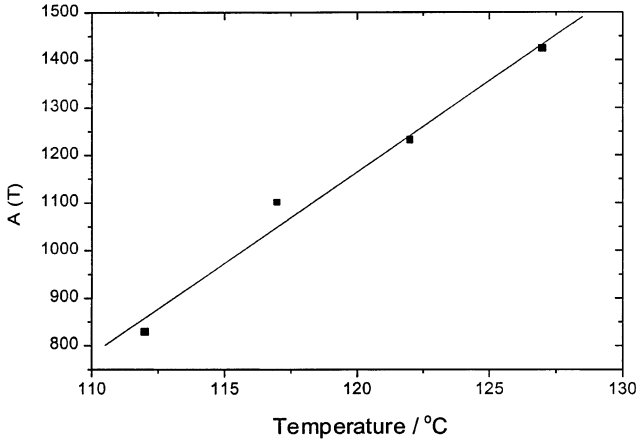


Fig. 10. The temperature dependence of the parameter $A$.

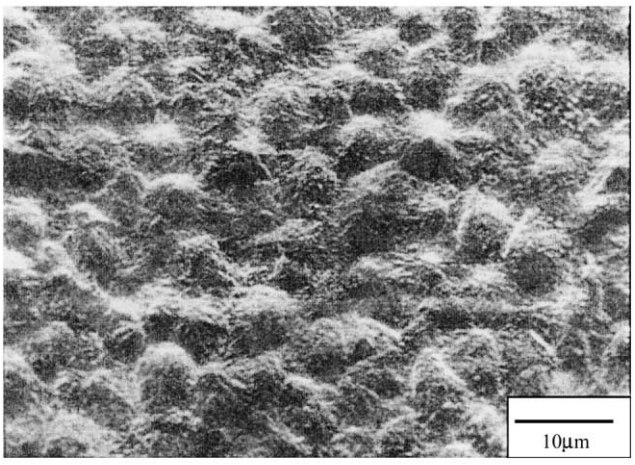


10 kV x 2,000

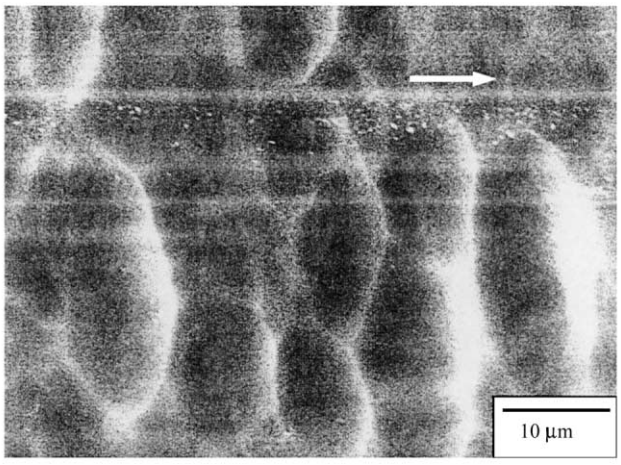


15 kV x 2,000

Fig. 11. (a) Spherulites of PET after annealing at 140°C for 0.5 h and KOH etching. (b) Deformed spherulites of PET formed by drawing to 50% extension followed by annealing at 140°C for 0.5 h and etching with KOH/methanol solution.

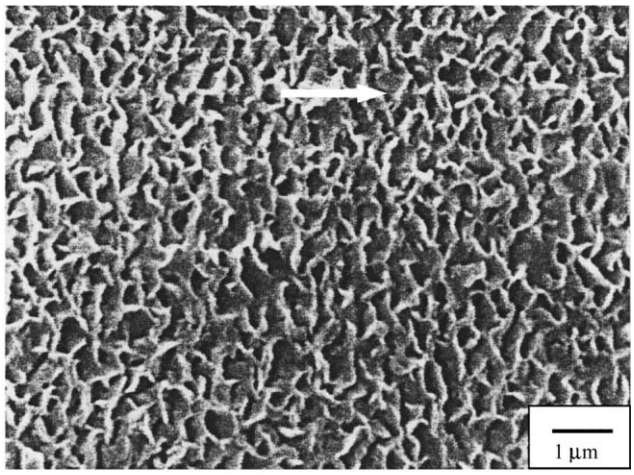


15 kV x 10,000

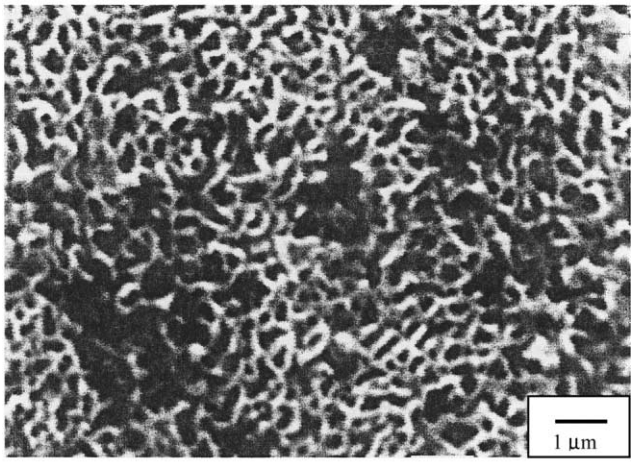


15 kV x 10,000

Fig. 12. (a) Microstructure of PET after drawing at 60°C to 200% elongation and *n*-propylamine etching. (b) Microstructure of PET after annealing at 140°C for 0.5 h and *n*-propylamine etching.

In the IR absorption spectrum of PET, the following assignments were adopted: the absorption band at 973 $cm^{-1}$ was assigned to be due to the $CH_2$ vibration mode of the *trans* conformers, for which the angle $\alpha = 34°$ [59], the absorption band at 896 $cm^{-1}$ to $CH_2$ vibration of the *gauche* conformers [5] but $\alpha$ is unknown. Similarly, the absorption band at 1340 $cm^{-1}$ has been assigned to $CH_2$ wagging mode of the glycol segments in the *trans* conformer [35] and the angle $\alpha = 21°$ [60]. The absorption band at 1337 $cm^{-1}$ corresponds to $CH_2$ wagging modes of the glycol segments in *gauche* conformation [61,62] but $\alpha$ is not known. The 1020 $cm^{-1}$ absorption band has been attributed to the in-plane bending of C–H bands of the benzene ring [60,63,64]. Since the band is not directly related to *trans* or *gauche* conformers, so the orientation of this band is representative of the overall orientation, $\alpha = 20°$ [43,46]. The 730 $cm^{-1}$ absorption band is due to the out-of-plane bending of the benzene ring C–H band, is representative of the overall orientation and $\alpha = 90°$ [61,62]. Similarly, the absorption bands at 749 and 1410 $cm^{-1}$ are associated with benzene ring vibration.

Although there are numerous IR absorption bands that exhibit dichroism in PET beside those mentioned, the bands at 973, 1340 and 1370 $cm^{-1}$ are strongly dichroic. Hence, they are usually used to follow changes in orientation, especially at low draw ratios, since most other peaks have dichroic ratios too close to unity to be measured precisely. Additionally, they do not absorb too strongly and by controlling the thickness to less than 20 μm, saturation of the absorption bands can be avoided.

From Fig. 13, the changes in the IR spectra with polarization angle can be seen in samples drawn to 200% at strain rate $3.3 \times 10^{-3}$ $s^{-1}$ at 75°C. On changing the polarization angle at interval of 30°, maximum and minimum absorbances were obtained at 0 and 90°, respectively. Absorption bands, at 973, 896, 1340 and 1337 $cm^{-1}$, in

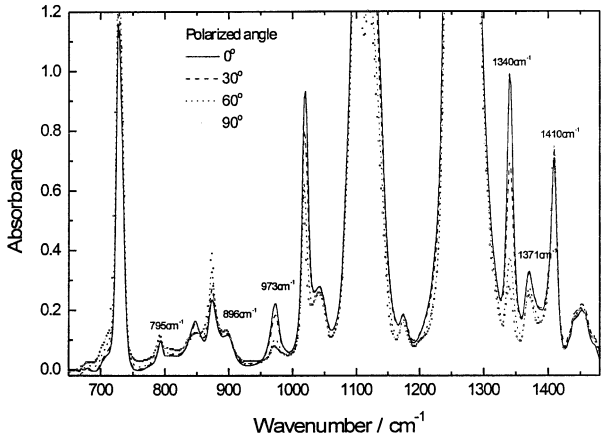


Fig. 13. Variations of IR absorbance with polarized light angle relative to draw direction.

particular, changed their intensity markedly. Following Eq. (6), the ratio of absorbance at 0 and 90° was used to define the dichroic ratio, but only at the highest draw ratios, i.e. $\lambda > 5$, the absorbances of the bands at 795 and 1410 $cm^{-1}$ exhibited any slight change with polarized beam angle. Based on this, the IR absorption intensities were normalized to these bands. Two pairs of bands at 973 and 896 $cm^{-1}$ and 1340 and 1337 $cm^{-1}$ were used to determine the degree of orientation and conformation changes on drawing from the Herman orientation function. It is clear from Fig. 14 that the concentration of the *trans* conformers, represented by the bands at 973 and 1340 $cm^{-1}$ were much larger than those of the *gauche* conformers, represented by bands 896 and 1337 $cm^{-1}$. Comparing Fig. 14 with Fig. 5, it can be seen that crystallization started immediately on drawing. This is at variance with the conclusions of LeBourvellec et al. [50] who observed a time lag between the onset of orientation and the beginning of crystallization at higher temperatures where molecular chain relaxations occur more quickly. Since the orientation of the *gauche* conformer, represented by the bands at 896 and 1371 $cm^{-1}$ was small. It contributed little to the overall orientation of the molecular chains, such that it could be neglected.

It is generally considered that two phases, i.e. crystalline and amorphous, exist in semicrystalline polymers [65], but it has been considered that three phases, i.e. crystalline which is composed entirely of *trans* conformer, amorphous containing a mixture of *trans* and *gauche* conformers, and a mesophase which is also composed of *trans* conformers only exist in strain-induced crystallized polymers [42,43,66]. The problem remains, however, in that the spectra of the *trans* isomer in the crystalline phase, amorphous phase and mesophase are sufficiently similar as not to be resolved directly by the presently available experimental techniques or by theory. Because of the uncertainties of the mesophase, this study preferred to adopt a two-phase model of crystalline and non-crystalline phases, the latter being the summation of the disoriented amorphous phase and the ordered mesophase. The fraction of crystallinity can be determined by DSC, as shown in Fig. 5. From the overall content of *trans* conformers measured by transmission IR spectroscopy, the *trans* content in the crystalline and non-crystalline phases can be determined separately.

Quantitative analysis of the IR spectrum was based on the application of the Beer–Lambert law, i.e.

$$A = \log_{10}\left(\frac{I_0}{I}\right) = \varepsilon c l \tag{8}$$

where $A$ is the absorbance, $I_0$ the intensity of the incident infrared radiation, $I$ the infrared radiation transmitted through the sample, $\varepsilon$ the molar absorption coefficient, $c$ the concentration of an absorbing species and $l$ the thickness of the sample.

Accordingly,

$$A_{973} = \varepsilon_{973} c_t l \tag{9}$$

$$A_{896} = \varepsilon_{896} c_g l \tag{10}$$

$$A_{795} = \varepsilon_{795} c_0 l \tag{11}$$

where the subscript refers to the wave number of the

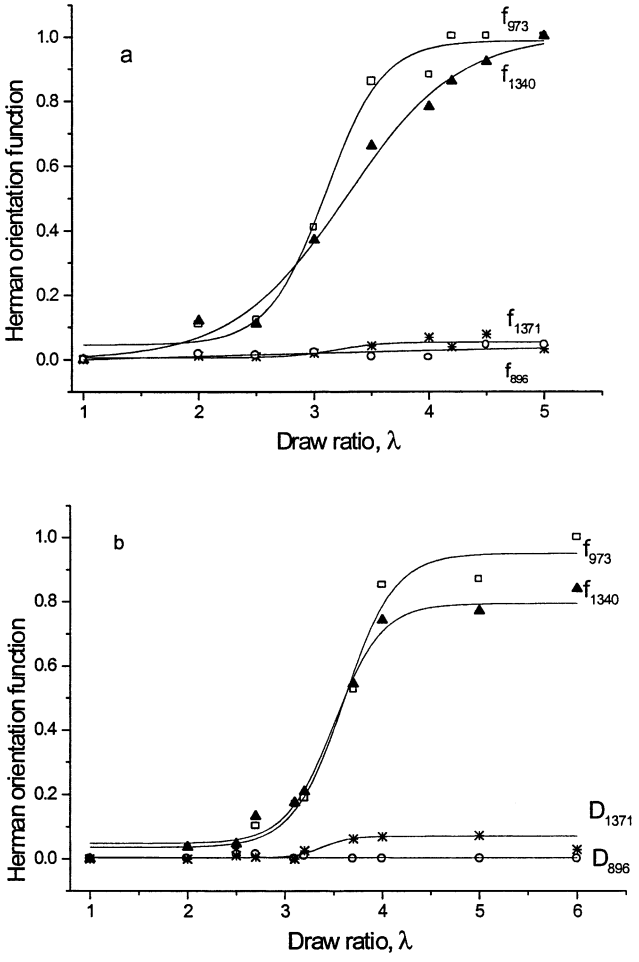


Fig. 14. Changes in the orientation degree of various absorption bands with draw ratios: (a) 75°C and strain rate $17 \times 10^{-3}\ s^{-1}$; (b) 75°C and strain rate $3.3 \times 10^{-3}\ s^{-1}$.

absorbance band, $c_t$ and $c_g$ the mole concentrations of *trans* and *gauche* conformers, respectively, and $c_0$ the total molar concentration of bulk PET.

$$\frac{A_{973}}{A_{795}} = \frac{\varepsilon_{973}}{\varepsilon_{795}}\left(\frac{c_t}{c_0}\right) = X_t\frac{\varepsilon_{973}}{\varepsilon_{795}} \tag{12}$$

$$\frac{A_{896}}{A_{795}} = \frac{\varepsilon_{896}}{\varepsilon_{795}}\left(\frac{c_t}{c_0}\right) = X_g\frac{\varepsilon_{896}}{\varepsilon_{795}} \tag{13}$$

Assuming

$$p_1 = \frac{\varepsilon_{795}}{\varepsilon_{973}} \quad \text{and} \quad p_2 = \frac{\varepsilon_{795}}{\varepsilon_{896}}$$

then

$$\frac{A_{973}}{A_{795}}\frac{\varepsilon_{795}}{\varepsilon_{973}} = X_t = \left(\frac{A_{973}}{A_{795}}\right)P_1 \tag{14}$$

and

$$\frac{A_{896}}{A_{795}}\frac{\varepsilon_{795}}{\varepsilon_{896}} = X_g = \left(\frac{A_{973}}{A_{795}}\right)P_2 \tag{15}$$

Furthermore,

$$X_t + X_g = 1 = p_1\frac{A_{973}}{A_{795}} + p_2\frac{A_{896}}{A_{795}} \tag{16}$$

Similarly, assuming

$$q_1 = \frac{\varepsilon_{1410}}{\varepsilon_{1340}} \quad \text{and} \quad q_2 = \frac{\varepsilon_{1410}}{\varepsilon_{1371}}$$

then

$$X_t + X_g = 1 = q_1\frac{A_{1340}}{A_{1410}} + q_2\frac{A_{1371}}{A_{1410}} \tag{17}$$

where $A$ is the absorbance of the band with no orientation [67], obtained from $A = 1/3(A_{\parallel} + 2A_{\perp})$. Here $A_{\parallel}$, $A_{\perp}$ are absorbances parallel and perpendicular to the drawn direction for each absorption band, respectively.

Eqs. (16) and (17) can be modified to

$$\frac{A_{795}}{A_{896}} = p_1\frac{A_{973}}{A_{896}} + p_2 \tag{18}$$

and

$$\frac{A_{1410}}{A_{1371}} = p_1\frac{A_{1340}}{A_{1371}} + p_2 \tag{19}$$

The values of $p_1$, $p_2$ and $q_1$, $q_2$ depended on the bands used. The values of the terms

$$p_1\frac{A_{973}}{A_{795}} \quad \text{and} \quad p_2\frac{A_{896}}{A_{795}}$$

and also

$$q_1\frac{A_{1340}}{A_{1410}} \quad \text{and} \quad q_2\frac{A_{1371}}{A_{1410}}$$

represented the *trans* and *gauche* conformer concentration, respectively. At 75°C and a strain rate of $17 \times 10^{-3}\ s^{-1}$, the values of $p_1$, $p_2$ and $q_1$, $q_2$ for each pair of bands are shown in Fig. 15. Similar analysis was carried out on samples drawn under different conditions of temperature and strain rate and for each pair of bands $p_1$, $p_2$ and $q_1$, $q_2$ separately determined from this the fraction of each isomer was calculated, see Figs. 16 and 17. Clearly, there was an equilibrium distribution of *trans* and *gauche* conformers in the initial amorphous PET ($\lambda = 1$) and the fraction of *trans* conformers was $0.10 \pm 0.01$, although different pairs of bands were used. The results were similar and consistent with the literature values measured by IR specular reflection technique [63].

Usually, an overall orientation, averaged over both amorphous and crystalline phases, can be determined directly from optical birefringence measurements [5,60]. In principle, certain infrared bands, such as 1020 and 730 $cm^{-1}$ can also be used to determine the overall orientation. Unfortunately, both of these bands are too strongly absorbing and

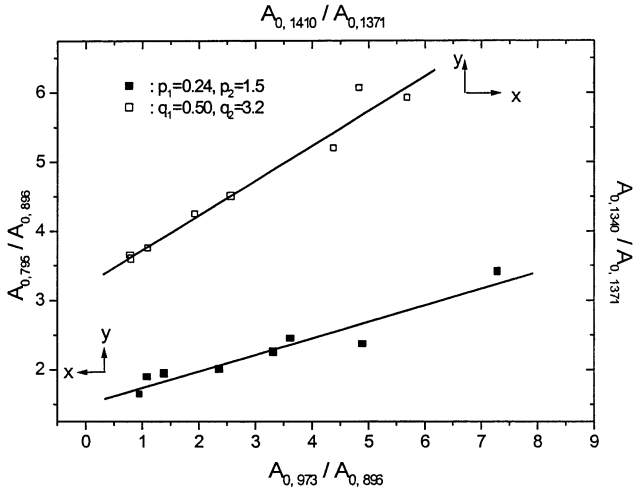


Fig. 15. Determination of the parameters $p_1$, $p_2$ and $q_1$, $q_2$ for PET drawn at 75°C at strain rate $17 \times 10^{-3}\ s^{-1}$.

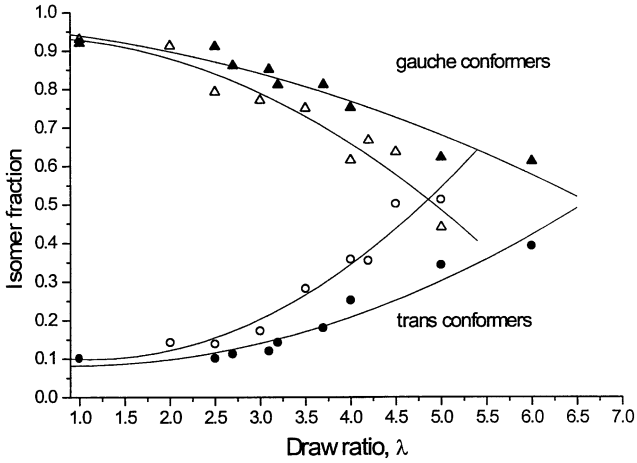


Fig. 16. Changes of the isomer fraction with draw ratio for PET drawing at 75°C (calculation based on bands at 973, 896 and 795 $cm^{-1}$).

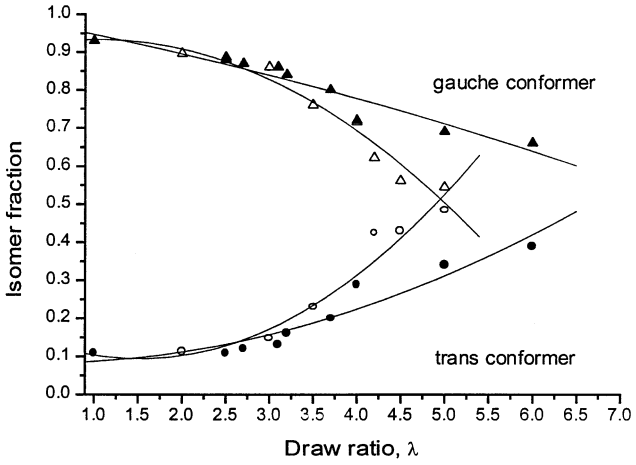


Fig. 17. Changes of the isomer fraction with draw ratio for PET drawing at 75°C (calculation based on bands at 1340, 1371 and 1410 $cm^{-1}$).

are easily saturated even at low draw ratio. Alternatively, the overall orientation can be calculated from [34,36]

$$f_{\text{overall}} = f_{trans}X_{trans} + f_{gauche}X_{gauche} \quad (20)$$

or,

$$f_{\text{overall}} = f_{\text{cryst}}X_{\text{cryst}} + f_{\text{non-cryst}}X_{\text{non-cryst}} \quad (21)$$

where $f$ denotes the orientation function and $X$ the weight fraction of the phase being considered. In this way, the overall orientation and the contribution of the crystalline and non-crystalline phases to the overall orientation can be separated, as shown in Figs. 18 and 19. In addition, the fraction of *trans* conformers in the crystalline and non-crystalline phases could be measured, as shown in Fig. 20. Similar results were obtained using the different absorption bands to an error of 3%, suggesting that the transmission IR technique using a polarizer was precise for characterizing polymer orientation.

It can be seen in Fig. 20 that in the PET film stretched at 75°C at a strain rate of $17 \times 10^{-3}\ s^{-1}$, the *trans* conformers

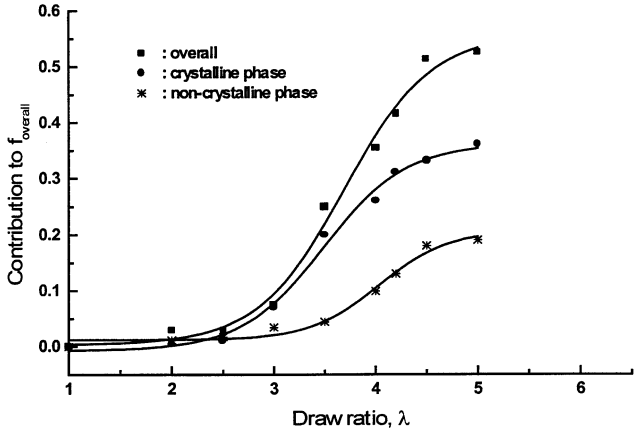


Fig. 18. The orientation contribution of the crystalline and non-crystalline phases to the overall orientation for PET film drawn at 75°C and strain rate $17 \times 10^{-3}\ s^{-1}$ (calculation based on bands at 973, 896 and 795 $cm^{-1}$).

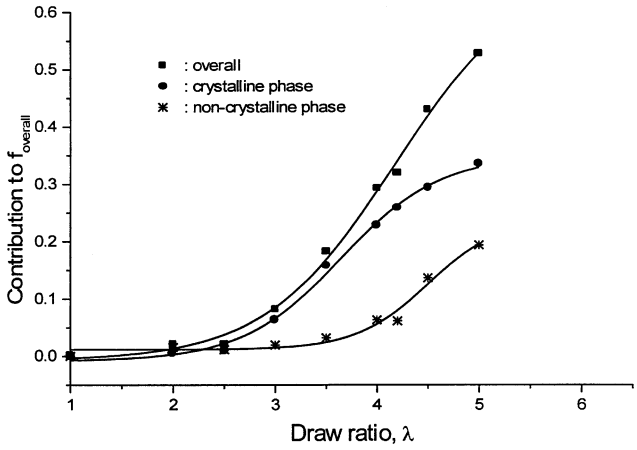


Fig. 19. The orientation contribution of the crystalline and non-crystalline phases to the overall orientation for PET film drawn at 75°C and strain rate $17 \times 10^{-3}\ s^{-1}$ (calculation based on bands at 1340, 1371 and 1410 $cm^{-1}$).

in the amorphous phase disappeared first by the production of crystallinity regions, as indicated by the overall decrease of the fraction of *trans* conformers in the non-crystalline phase. With increasing draw ratio, more and more of the *gauche* conformers convert to *trans*, part of which is in that crystalline and part in the non-crystalline phase. The crystallinity develops rapidly between $\lambda$ of 2–4 and approaches saturation at $\lambda = 4$. Beyond $\lambda = 4$, the *trans* content of the non-crystalline phase increases continuously with the content of *trans* conformers in the crystalline phase constant with further drawing.

Similarly, on uniaxially drawing at the strain rate of $3.3 \times 10^{-3}\ s^{-1}$, the orientation contribution of the crystalline and non-crystalline phases to the overall orientation of PET was obtained, as shown in Fig. 21. In addition, the *trans* contents in crystalline and non-crystalline phases are shown in Fig. 22. Compared with Fig. 20, it can be seen that the strain rate had no obvious effect on the orientation of the non-crystalline phase initially up to $\lambda = 4$, no matter which strain rate was used, i.e. $17 \times 10^{-3}$ or $3.3 \times 10^{-3}\ s^{-1}$.

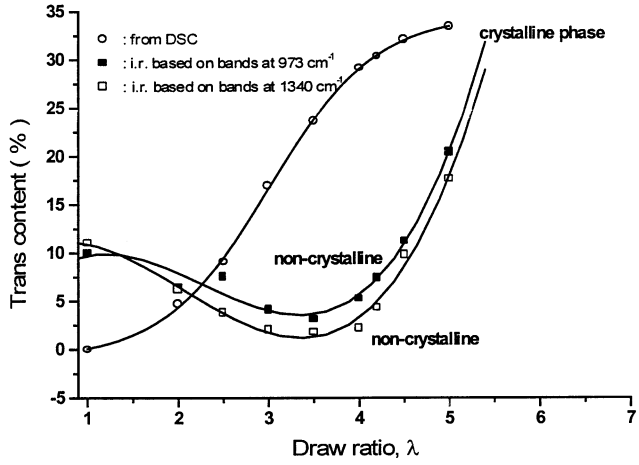


Fig. 20. Distribution of *trans* conformers in crystalline and non-crystalline phases of PET drawn at 75°C and strain rate $17 \times 10^{-3}\ s^{-1}$.

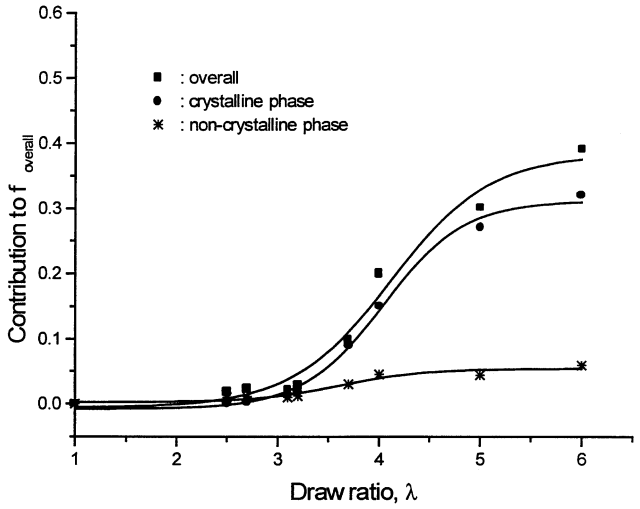


Fig. 21. Orientation contribution of the crystalline and non-crystalline phases to the overall orientation for PET film drawn at 75°C and strain rate $3.3 \times 10^{-3}\ s^{-1}$ (calculation based on bands at 973, 896 and 795 $cm^{-1}$).

Beyond $\lambda = 4$ and drawing at $17 \times 10^{-3}\ s^{-1}$ led to a rapid increase in the *trans* contents of the non-crystalline phase, possibly due to the development of a mesophase with increasing draw ratio. Whereas, drawing at a strain rate of $3.3 \times 10^{-3}\ s^{-1}$ gave no obvious change in the *trans* contents of the non-crystalline up to $\lambda = 6$. While the *trans* contents in the crystalline phase appeared to increase sigmoidally with the increasing draw ratio, it eventually reached saturation, as did drawing at $17 \times 10^{-3}\ s^{-1}$ but at a slower rate, as previously shown in Fig. 5. This implies that drawing at this strain rate gave sufficient time for the oriented molecular chain segments in non-crystalline phase to relax almost completely, only part of the oriented molecular chain segments became stabilized on attaining crystal structures.

### 3.3. Relaxation of orientation

Initial investigations on relaxation were carried out by annealing at 75°C sample drawn at $17 \times 10^{-3}\ s^{-1}$ to $\lambda = 2.5$. On annealing, the absorbances of the bands at 896, 973, 1340 and 1371 $cm^{-1}$ changed, see Fig. 23. After 5 min, the orientation function for the bands at 973 $cm^{-1}$ reduced from 0.12 (without annealing) to 0.10, and 1340 $cm^{-1}$ from 0.11 to 0.10. It would appear that orientation was reduced by stress relaxation.

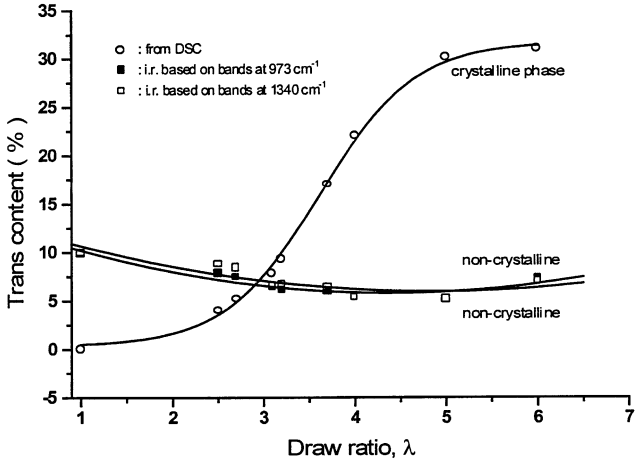


Fig. 22. Distribution of *trans* conformers in crystalline and non-crystalline phases of PET drawn at 75°C, strain rate $3.3 \times 10^{-3}\ s^{-1}$.

## 4. Conclusions

Our studies have focused on the effects of three main parameters, i.e. elongation, strain rate and temperature on orientation, relaxation and crystallization in PET. It was found that:

1. At the same temperature, the strain-induced crystallization rate is much faster than thermally induced one and uniaxially drawing results in crystallization below $T_g$, which never happens in the absence of stress. This has been attributed to the entropy of extension, which lowers the free energies for nucleation and crystal growth and hence increases the driving force for crystallization. Avrami analysis indicates thermally induced crystallization and strain-induced crystallization have different nucleation and growth mechanisms, which is in consistent with the morphology change from spherulites to ellipsoids, finally with increasing orientation degree to that of extended chain crystals, and 'shish-kebab'

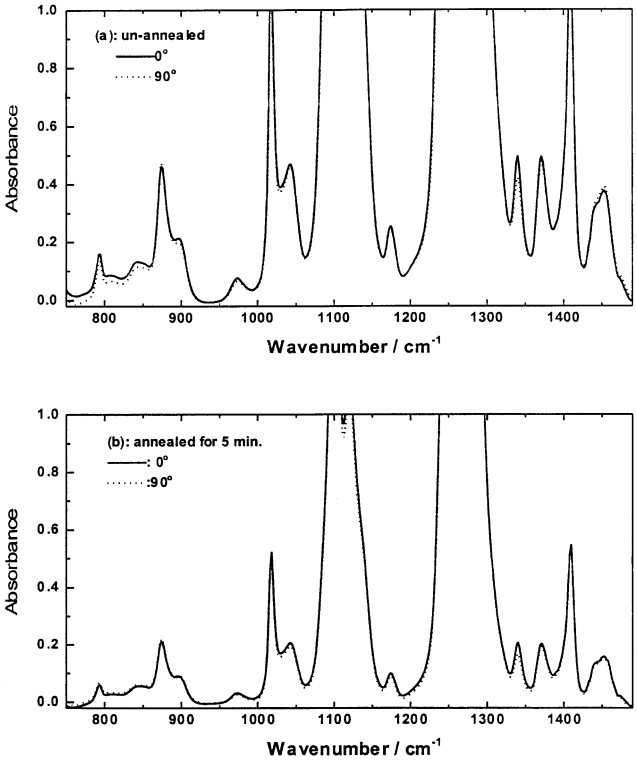


Fig. 23. Polarizability function spectra from PET film drawn at 75°C and strain rate $17 \times 10^{-3}\ s^{-1}$(without and with further annealing).

structure with row nucleation of folded crystals. The effect of initial orientation on crystallization kinetics can be approximately described by Ziabicki empirical equation.

2. Increasing elongation invariably leads to increased levels of orientation and crystallinity. When uniaxially drawing starts, molecular chain segments begin to align in the drawing direction. Firstly, orientation happens and with the increase of orientation, the mobility of molecular chains progressively increase. Further increasing elongation gives rise to three competing processes, i.e. the orientation degree in the non-crystalline region continues to increase, possibly due to the development of 'mesophase'; the oriented molecular chain segments develop into crystalline regions and the orientated molecular chain segments relax due to the increased mobility. However, once crystals form, the mobility of molecular chain and segments in the non-crystalline region begins to decrease as crystals can act as cross-links for the non-crystalline matrix and hinder the relaxation of chain segments. Slight crystallinity reduces the relaxation rate of molecular chain segments markedly.
3. Strain rate affects the orientation and the relaxation significantly, especially in hot-drawing in that higher strain rate enables less time for the relaxation of molecular chain segments, thus promotes orientation and crystallization. Lower strain rate supplies more time for the relaxation of molecular chain segments. Although at higher temperature (e.g. $>90°C$) and relatively lower strain rate (e.g. $<1\ s^{-1}$), when the whole molecular chains of PET exhibit great elongation, the orientation degree of chain segments keeps very low because the relaxation of chain segments proceed more quickly than the whole molecular chains.
4. At a given strain rate and elongation, the increase of temperature causes a decrease in the degree of orientation and crystallinity. This suggests that increasing temperature reduces the effectiveness of stress in orienting the chain and increasing the developing the crystallization, as it increases the relaxation rate of molecular chain segments by increasing the mobility of chain segments. Essentially, the onset and development of crystallinity for drawing under a given condition and the final orientation degree attained in a sample depend on the relative rates of relaxation time of molecular chain segments and crystallization half time.

## References


[1] Kawaguchi T. J Appl Polym Sci 1961;16:482.
[2] Misra A, Stein RS. J Polym Sci, Polym Phys Ed 1979;17:235.
[3] Jabarin SA. Polym Engng Sci 1992;32:1341.
[4] Rietsch F, Duckett RA, Ward IM. Polymer 1979;20:1133.
[5] Padibjo SR, Ward IM. Polymer 1983;24:1103.
[6] Huang B, Ito M, Kanamoto I. Polymer 1994;35:1210.
[7] Spruiell JE, McCord DE, Beuerlein RA. Trans Soc Rheol 1972;16:535.
[8] DeVries AJ, Bonnebat C. Polym Engng Sci 1976;16:93.
[9] Jabarin SA. Polym Engng Sci 1984;24:376.
[10] Alfonso GC, Verdona MP, Wasiak A. Polymer 1978;19:711.
[11] Wasiak A. Colloid Polym Sci 1981;259:135.
[12] Smith FS, Steward RD. Polymer 1974;15:283.
[13] Biangardi HJ, Zachmann HG. J Polym Sci, Polym Symp 1977;58:169.
[14] Stein RS. Polym Engng Sci 1976;16:153.
[15] Gupte KM, Motz H, Schultz JM. J Polym Sci, Polym Phys Ed 1983;21:1927.
[16] Sun T, Pereira JRC, Porter RS. J Polym Sci, Polym Phys Ed 1984;22:1163.
[17] Peszkin P, Schultz JM. J Polym Sci, Polym Phys Ed 1986;24:2591.
[18] Desai P, Abhiraman AS. J Polym Sci, Polym Phys Ed 1988;26:1657.
[19] Desai P, Abhiraman AS. J Polym Sci, Polym Phys Ed 1989;27:2469.
[20] LeBourvellec G, Monnerie L, Jarry JP. Polymer 1987;28:1712.
[21] Lapersonne P, Bower DI, Ward IM. Polymer 1992;33:1277.
[22] Salem DR. Polymer 1992;33:3183.
[23] Farrow G, Ward IM. Polymer 1960;1:330.
[24] Chu CM, Wilkes GL. J Macromol Sci 1974;B10(2):231.
[25] Nobbs JH, Bower DI, Wards IM. Polymer 1976;17:25.
[26] Havens JR, Van der Hart DL. Macromolecules 1985;18:1663.
[27] Dargent E, Grenet J, Aurray X. J Therm Anal 1994;41:1409.
[28] Lapersonne P, Tassin JF, Monnierie L. Polymer 1994;35:2192.
[29] Ajji A, Guèvremont J, Cole KC, Dumoulin MM. Polymer 1996;37:3707.
[30] Schmidt PG. J Polym Sci 1963;A-1:1271.
[31] Fina LJ, Koeing JE. J Polym Sci, Part B: Polym Phys 1986;24:1509.
[32] Walls DJ, Coburn JC. J Polym Sci, Polym Phys Ed 1992;30:887.
[33] Walls DJ. Appl Spectrosc 1991;45:1193.
[34] Lofgren EA, Jabarin SA. J Appl Polym Sci 1994;51:1251.
[35] Ajji A, Cole KC, Dumoulin MM, Brisson J. Polymer 1995;36:4023.
[36] Cole KC, Guèvremont J, Ajji A, Dumoulin MM. Appl Spetrosc 1994;48:1513.
[37] Guèvremont J, Ajji A, Cole KC, Dumoulin MM. Polymer 1995;36:3385.
[38] Chow TS, Van Laeken AC. Polymer 1991;32:1799.
[39] Okazaki I, Wunderlich B. J Polym Sci, Polym Phys 1996;34:2941.
[40] Song R, Lin X, Gao JG, Fan QR. Polym Bull 1998;40:773.
[41] Hay JN, Mills PJ. Polymer 1982;23:1380.
[42] Salem DR. Polym Engng Sci 1999;39(12):2419.
[43] Salem DR. Polymer 1994;35:771.
[44] Blunder DJ, MacKerron DH, Fuller W, Mahendrasingam A, Martin C, Oldman RJ, Rule RJ, Riekel C. Polymer 1996;37:3303.
[45] Aref-Azar A, Arnoux F, Biddlestone F, Hay JN. Thermochim Acta 1996;273:217.
[46] Qian RY, Fan QR, Guan JY. Acta Polym Sin 1997;3:343.
[47] Gilli R, Canetti M, Sadocco P, Seves A, Vicini L. J Polym Sci, Polym Phys Ed 1983;21:717.
[48] Göschel U. Polymer 1996;18:4049.
[49] Mehment-Alkan AA, Hay JN. Polymer 1992;33:3527.
[50] LeBourvellec G, Monnerie L, Jarry JP. Polymer 1986;27:856.
[51] Avrami MJ. Chem Phys 1939;7:1103.
[52] Avrami MJ. Chem Phys 1940;8:212.
[53] Hay JN. Flow-induced crystallization in polymer systems. New York: Gordon and Breach, 1979. p. 69–95.
[54] Ziabicki A. Colloid Polym Sci 1974;252:207.
[56] Stein RS. Polym Engng Sci 1976;16:153.
[57] Pennings AJ, Pijpers MFJ. Macromolecules 1970;3:261.
[58] Pennings AJ, Pijpers MFJ. Kolloid-Z Z Polym 1970;236:99.
[59] Spiby P, O'Nell MA, Duckett RA, Ward IM. Polymer 1992;21:4479.
[60] Ajji A, Cole KC, Dumoulin MM, Ward IM. Polym Engng Sci 1997;37(11):1801.

[61] Matthews RG, Ajji A, Dumoulin MM, Prud'Homme RE. Polym Engng Sci 1999;39(12):2377.
[62] Bahl SK, Cornell DD, Boerio FJ, McGraw GE. J Polym Sci, Polym Lett Ed 1974;12:13.
[63] Cunningham A, Ward IM. Polymer 1974;15:749.
[64] Hutchinson IJ, Ward IM, Willis HA, Zichy V. Polymer 1980;21:55.
[65] Quintanilla L, Rodriguez-Cabello JC, Jawhari T, Pastor JM. Polymer 1993;34:3787.
[66] Ajji A, Guèvremont J, Cole KC, Dumoulin MM. Polymer 1996;16:3707.
[67] Fina LJ, Koenig JL. J Polym Sci, Part B 1986;24:2525.